Available online at www.sciencedirect.com
SCIENCE DIRECT®
Computer Physics Communications 168 (2005) 141–158
Computer Physics Communications
www.elsevier.com/locate/cpc

A transport simulation code for inertial confinement fusion relevant laser–plasma interaction

S. Weber [a,b,*], P.-H. Maire [a], R. Loubère [c], G. Riazuelo [b], P. Michel [b,d], V. Tikhonchuk [a], J. Ovadia [e]

[a] *CELIA, Université Bordeaux 1, 33405 Talence, France*
[b] *CEA/DAM/DIF/DPTA, BP 12, 91680 Bruyères-le-Châtel, France*
[c] *Los Alamos National Laboratory, Group T-7, Los Alamos, NM 87544, USA*
[d] *LULI, École Polytechnique, 91128 Palaiseau, France*
[e] *CEA/DAM/CESTA/DEV, 33114 Le Barp, France*

Revised 27 January 2005; accepted 27 January 2005

Available online 12 May 2005

Abstract

We present a code for the simulation of laser–plasma interaction processes relevant for applications in inertial confinement fusion. The code consists of a fully nonlinear hydrodynamics in two spatial dimensions using a Lagrangian, discontinuous Galerkin-type approach, a paraxial treatment of the laser field and a spectral treatment of the dominant non-local transport terms. The code is fully parallelized using MPI in order to be able to simulate macroscopic plasmas.

One example of a fully nonlinear evolution of a laser beam in an underdense plasma is presented for the conditions previewed for the future MegaJoule laser project.

PACS: 02.70.Dh; 47.11.+j; 52.35.Tc; 52.38.-r; 52.65.Kj; 52.57.-z

Keywords: Laser–plasma interaction; Lagrangian hydrodynamics; Discontinuous Galerkin method; Non-local transport; Inertial confinement fusion

1. Large-scale laser–plasma interaction (LPI) in ICF context

The forthcoming large-scale projects devoted to inertial confinement fusion (ICF) in France (CEA-LMJ) and the US (LLNL-NIF) require a predictive modeling of the relevant physical processes. There are three levels of

* Corresponding author.
E-mail address: weber@celia.u-bordeaux1.fr (S. Weber).

0010-4655/$ – see front matter
doi:10.1016/j.cpc.2005.01.017

modeling currently implemented in laser fusion studies. The macroscopic modeling describes the target acceleration, the fuel compression, the ignition of fusion reactions and the energy yield. However these codes are too coarse-grained to account for electromagnetic effects and the laser energy deposition is often treated as a boundary condition. The microscopic codes account for particle kinetics and full electromagnetic effects but they are restricted to local descriptions at the level of a few hundred cubic microns in space and a few picoseconds in time.

The present code belongs to the third category of codes, operating on the mesoscopic level, which constitute a bridge between the microscopic "elementary" physics and the practical needs of target design. The purpose of these codes is to provide a realistic description of laser–plasma interaction (LPI) and to optimize the laser energy deposition for fusion studies. The term "realistic" in this case implies macroscopic plasma volumes of the order of one mm^3 and laser exposure times of the order of several nanoseconds [17,21].

There are three basic ingredients for such a simulation tool: a reduced paraxial treatment of the incident laser beam, a nonlinear hydrodynamics for the plasma response and a valid approach accounting for the kinetic effects (wave and particle interactions).

The assumption of quasi-neutrality for the plasma implies that the equations of the plasma as a fluid are given by the standard equations of ideal gas dynamics. For present considerations of interest the presence of self-consistent electric and magnetic fields plays no role. However, due to the specific conditions encountered in many LPI applications, one has to take into account certain kinetic effects within the hydrodynamic models. These kinetic effects present themselves as modifications of the usual transport coefficients induced by a large mean free path of the particles and by coupling of the plasma to the laser field.

The most advanced mesoscopic LPI code is pF3D [1] developed over the last 10 years in the Lawrence Livermore National Laboratory. It accounts for many physical effects such as laser propagation, auto-focalization, stimulated forward and backward Raman and Brillouin scattering, etc. The hydrodynamical part of this code is fully 3-dimensional and accounts for several models of non-local heat transport and some other effects. Our code is more limited. It is intended above all for describing effects due to laser propagation. It does not account for backscattering and the hydrodynamical plasma response is 2-dimensional in the plane transverse to the laser beam axis. However, this code has several attractive features at the level of the plasma response description which offers a more efficient treatment of the laser–plasma interactions. In particular, the numerical scheme allows for a much smaller number of mesh-points while maintaining the precision compared to standard schemes. Also no numerical oscillations appear at the fronts of shocks and at strong gradients. These features are very favorable for treating strongly inhomogeneous laser fields and large plasma volumes. Since the main coupling terms between the plasma and the laser are acting in the plane transverse to the propagation direction of the laser beam, the hydrodynamic module is 2-dimensional in our code. The disadvantage being that plasma flow along the laser axis cannot be accounted for. The numerical scheme allows without problem its extension to the third direction and can also be generalized to multi-species plasmas. However, these features would undermine the performance of the code.

We consider the present version of the code as a basic one which contains sufficient physics for analysis of current experiments and predictive modeling of LPI for fusion research.

The outline of the remaining paper is as follows. Section 2 explains the novel numerical method used for the hydrodynamics. Section 3 presents the global formulation of the model: the parabolic electromagnetic equation and the non-local Navier–Stokes equations, followed in Section 4 by the issue of the non-local transport. Finally, Section 5 presents some results of a recent application of the code in the strongly nonlinear regime.

2. Discontinuous Galerkin approach for plasma hydrodynamics

Laser beams for the present ICF studies have a complicated spatio-temporal structure on the time scale of a few ps and a spatial scale of a few μm with intensity variations more than one order of magnitude. Such inhomogeneities of the laser electromagnetic field can be considered as local hot spots or speckles which have a random statistical

distribution. The modeling of speckles in the context of laser–plasma interaction gives rise to strong gradients in the density. The induced flow is characterized by local non-stationary compression and rarefaction. Therefore a numerical method is required which allows to resolve these gradients with a high precision and with a minimal number of mesh points.

For this purpose a Lagrangian method is used to solve the nonlinear hydrodynamic equations [14,15] which describe the plasma response. In contrast to most Lagrangian approaches, the method used here represents all spatial derivatives entirely in Lagrangian variables. This implies that one has to follow the time evolution of the Jacobian relating the Eulerian and Lagrangian spaces. The space discretization is based upon an original discontinuous Galerkin method which uses as a basis the Bernstein polynomials. Instead of solving for the variables themselves, one uses the moments of the variables with respect to the Bernstein polynomials. The moments method induces some weak intrinsic numerical diffusion which allows us to avoid the use of the classical slope limiter and suppresses spurious numerical oscillations. At the interfaces between two adjacent computational cells the Riemann problem is solved by using the classical Godunov solver. This approach allows a straightforward generalization to higher orders of precision. At present our code works at third order.

The coupling to the laser field gives rise to several sources (ponderomotive force, heating and transport terms) which are calculated in the Eulerian framework and which have to be projected onto the Lagrangian mesh. These terms are constructed as continuous sources over the whole computational domain using the corresponding moments on the Bernstein basis.

In the following we present in some detail the numerical scheme in one spatial dimension (1D), followed by a general outline of the method in two dimensions.

2.1. The 1D numerical scheme

2.1.1. Gas dynamic equations in Lagrangian coordinates

We consider a 1D flow in planar geometry, characterized by the density ρ, velocity u, pressure P and the total energy $e = u^2/2 + \varepsilon$, where ε denotes the internal energy. A perfect gas law for the equation of state (without loss of generality) is assumed: $P = (\gamma - 1)\rho\varepsilon$, where γ is the polytropic constant for a perfect gas. One can express the conservation of mass, momentum and total energy in the Lagrangian framework as follows:

$$\begin{cases} \partial_t(J) - \partial_x u = 0, \\ \partial_t(\rho J) = 0, \\ \partial_t(\rho J u) + \partial_x P = 0, \\ \partial_t(\rho J e) + \partial_x(P u) = 0, \quad \text{with } P = (\gamma - 1)\rho(e - \frac{1}{2}u^2), \end{cases} \tag{1}$$

where x denotes the Lagrangian coordinate which is the initial position of the Eulerian coordinate X; X and x are connected by the ordinary differential equation:

$$\partial_t X = u\big(X(t), t\big), \quad \text{with } X(0) = x, \tag{2}$$

which describes the particle paths. Here $J(x,t)$ is the Jacobian of the map $x \to X(x,t)$, i.e. $J = \partial_x X$. We solve the above system for $x \in \omega = [x_f, x_l]$ and $t \in [0, T]$. The boundary conditions are of two types: either the pressure or the velocity is imposed for $x = x_l$ and $x = x_f$. A set of initial conditions for the flow variables is given and for the Jacobian we impose $J(x,0) = 1$. In order to discretize the system (1) we define a subdivision of ω: $x_f = x_1 < \cdots < x_i < \cdots < x_{I+1} = x_l$ with $\Delta x_{i+1/2} = x_{i+1} - x_i$ and a subdivision of $[0, T]$: $0 = t_1 < \cdots < t_n < \cdots < t_{N+1} = T$ with $\Delta t = t_{n+1} - t_n$. The spatial discretization is based upon the Galerkin discontinuous method which uses a basis of Bernstein polynomials.

2.1.2. Bernstein polynomials

Let $\omega_{i+1/2} = [x_i, x_{i+1}]$ be a given cell of the mesh and x a point in $\omega_{i+1/2}$. We define the barycentric coordinates of x:

$$\lambda_1(x) = \frac{x_{i+1} - x}{x_{i+1} - x_i}, \quad \text{and} \quad \lambda_2(x) = \frac{x - x_i}{x_{i+1} - x_i}, \tag{3}$$

where λ_1 and λ_2 are positive functions of x and $\lambda_1(x) + \lambda_2(x) = 1$. The set $\{\lambda_1, \lambda_2\}$ is a basis of $P_1(\omega_{i+1/2})$—the set of polynomials of the order lower or equal to one. The definition of the Berstein polynomials of order K is straightforward using the binomial development of $(\lambda_1 + \lambda_2)^K$. For $k = 0 \dots K$ one considers the polynomial

$$\sigma_k^{(K)}(x) = C_K^k \lambda_1^k(x) \lambda_2^{K-k}(x), \tag{4}$$

where $C_K^k = \frac{K!}{k!(K-k)!}$. The set $\{\sigma_k^{(K)}\}_{k=0\dots K}$ is a basis of $P_K(\omega_{i+1/2})$—the set of polynomials of order lower or equal to K. These polynomials verify the following fundamental properties: for $k = 0 \dots K$ and $x \in \omega_{i+1/2}$

$$\begin{cases} \sigma_k^{(K)}(x) \geqslant 0, \\ \sum_{k=0}^K \sigma_k^{(K)}(x) = 1, \\ \int_{x_i}^{x_{i+1}} \sigma_k^{(K)}(x)\,\mathrm{d}x = \frac{\Delta x_{i+1/2}}{K+1}, \\ \sigma_k^{(K)}(x_i) = \delta_{k0}, \quad \sigma_k^{(K)}(x_{i+1}) = \delta_{kK}, \end{cases} \tag{5}$$

where δ_{kl} is the Kroenecker symbol ($\delta_{ll} = 1$ and $\delta_{kl} = 0$ for $k \neq l$). For $K = 2$ we have the following basis of $P_2(\omega_{i+1/2})$: $\sigma_0(x) = \lambda_1(x)^2$, $\sigma_1(x) = 2\lambda_1(x)\lambda_2(x)$ and $\sigma_2(x) = \lambda_2(x)^2$.

This Bernstein basis enables us to construct a polynomial approximation of a function on $\omega_{i+1/2}$ for any order K in the following way. Let $\phi(x)$ be a function on $\omega_{i+1/2}$, then we define its kth moment as:

$$M_{k,\phi} = \int_{x_i}^{x_{i+1}} \sigma_k^{(K)}(x)\phi(x)\,\mathrm{d}x. \tag{6}$$

One notices that $\sum_{k=0}^K M_{k,\phi} = \int_{x_i}^{x_{i+1}} \phi(x)\,\mathrm{d}x$. There are several ways to construct a polynomial approximation of order K. The most obvious one uses a projection of ϕ onto the space $P_K(\omega_{i+1/2})$ with the Bernstein basis: each moment of the function ϕ is equal to the moment of its polynomial approximation. Then we need to solve a linear system in order to compute the $K + 1$ components of ϕ on the Bernstein basis.

This method however has a major drawback: the lack of positivity, i.e. if ϕ is positive on $\omega_{i+1/2}$, its polynomial approximation might be somewhere negative. For our purposes positivity is a crucial need (the density, pressure, energy are positively defined functions). Thus one has to design a polynomial approximation which preserves positivity in a natural way. We construct $\hat{\phi}$ as:

$$\hat{\phi}(x) = \sum_{k=0}^K \hat{\phi}_k \sigma_k^K(x), \quad \text{with } \hat{\phi}_k = \frac{M_{k,\phi}}{M_{k,1}}, \tag{7}$$

where $M_{k,1} = \int_{x_i}^{x_{i+1}} \sigma_k^{(K)}(x)\,\mathrm{d}x$. In this way the positivity is guaranteed and one has as well a conservation of the mean value of ϕ:

$$\int_{x_i}^{x_{i+1}} \sigma_k^{(K)}(x)\hat{\phi}(x)\,\mathrm{d}x = \sum_{k=0}^K M_{k,\phi} = \int_{x_i}^{x_{i+1}} \sigma_k^{(K)}(x)\phi(x)\,\mathrm{d}x. \tag{8}$$

Moreover, this approximation adds a small amount of numerical diffusion which enhances the stability of the scheme.

2.1.3. Spatial discretization

The system (1) can be put in a more concise form:

$$\partial_t(J\phi) + \partial_x F(\phi) = 0, \tag{9}$$

where the vector $\phi = \{1, \rho, \rho u, \rho e\}$ and the vector of fluxes is defined as: $F = \{-u, 0, -P, Pu\}$. In the context of the discontinuous Galerkin method, the vector ϕ is approximated by a polynomial in each cell $\omega_{i+1/2}$ and this approximation is discontinuous at the cell boundaries. Thus, the spatial derivative $\{\partial_x\}$ has to be considered in the sense of distributions, i.e. it is equal to the classical derivative almost everywhere, except at the discontinuity points, where it is equal to the Dirac function times the jump of the function at these points. Thus for the cell $\omega_{i+1/2}$ we have:

$$\{\partial_x F(\phi)\} = \partial_x F(\phi) + \big[F(\phi_i^+) - F(\phi_i^\star)\big]\delta_{x_i} + \big[F(\phi_{i+1}^\star) - F(\phi_{i+1}^-)\big]\delta_{x_{i+1}}, \tag{10}$$

where $\phi_i^\pm = \lim_{x\to x_i^\pm}\phi(x)$ and $\phi_i^\star$ is the value which depends on the left- and right-hand side values (ϕ_i^-, ϕ_i^+) of ϕ, i.e. $\phi_i^\star$ is the solution of the classical Riemann problem. After multiplying Eq. (10) by $\sigma_k^{(K)}$ and integrating it over the cell $\omega_{i+1/2}$ one obtains:

$$\begin{aligned} &d_t M_{k,J\phi} + \int_{x_i}^{x_{i+1}} \partial_x F(\phi)\sigma_k^{(K)}(x)\,\mathrm{d}x + \big[F(\phi_i^+) - F(\phi_i^\star)\big]\sigma_k^{(K)}(x_i) \\ &\quad + \big[F(\phi_{i+1}^\star) - F(\phi_{i+1}^-)\big]\sigma_k^{(K)}(x_{i+1}) = 0. \end{aligned} \tag{11}$$

The integration by parts for the second term of the left-hand side leads to:

$$d_t M_{k,J\phi} - \int_{x_i}^{x_{i+1}} F(\phi)\partial_x\sigma_k^{(K)}(x)\,\mathrm{d}x + F\big(\phi_{i+1}^\star\big)\delta_{kK} - F\big(\phi_i^\star\big)\delta_{k0} = 0. \tag{12}$$

In order to compute the integral term, one replaces $F(\phi)$ by its polynomial approximation:

$$F(\phi) = \sum_{l=0}^{K} F(\hat{\phi}_l)\sigma_l^{(K)}(x). \tag{13}$$

Introducing a matrix D with coefficients:

$$D_{kl} = \int_{x_i}^{x_{i+1}} \partial_x\sigma_k^{(K)}(x)\sigma_l^{(K)}(x)\,\mathrm{d}x, \tag{14}$$

one obtains:

$$d_t M_{k,J\phi} - \sum_{l=0}^{K} D_{kl}F(\hat{\phi}_l) + F\big(\phi_{i+1}^\star\big)\delta_{kK} - F\big(\phi_i^\star\big)\delta_{k0} = 0. \tag{15}$$

The computation of the matrix D has to be performed just once and is independent of the mesh. For $K = 2$ we have the following values:

$$D = \begin{pmatrix} -\frac{1}{2} & -\frac{1}{3} & -\frac{1}{6} \\ \frac{1}{3} & 0 & -\frac{1}{3} \\ \frac{1}{6} & \frac{1}{3} & \frac{1}{2} \end{pmatrix}. \tag{16}$$

2.1.4. Time discretization

We use the classical two step Runge–Kutta method for the time discretization of Eq. (15):

- first step:

$$M_{k,J\phi}^{(n,1)} = M_{k,J\phi}^{n} + \Delta t\left[\sum_{l=0}^{K} D_{kl} F(\hat{\phi}_l^n) - \left\{F(\phi_{i+1}^{\star n})\delta_{kK} - F(\phi_i^{\star n})\delta_{k0}\right\}\right],$$

- second step:

$$M_{k,J\phi}^{(n,2)} = M_{k,J\phi}^{(n,1)} + \Delta t\left[\sum_{l=0}^{K} D_{kl} F(\hat{\phi}_l^{(n,1)}) - \left\{F(\phi_{i+1}^{\star(n,1)})\delta_{kK} - F(\phi_i^{\star(n,1)})\delta_{k0}\right\}\right].$$

One obtains order 2 precision with:

$$M_{k,J\phi}^{n+1} = \frac{1}{2}\left(M_{k,J\phi}^{n} + M_{k,J\phi}^{(n,2)}\right).$$

In the above equations the superscript n denotes the value of the function at the time t_n.

2.1.5. Computation of $\hat{\phi}_k$

Knowing the moments $M_{k,J\phi}$ for $\phi = 1, \rho, \rho u, \rho e$, one computes the so-called hat components in the following way:

$$\begin{cases} \hat{\rho}_k = \frac{M_{k,J\rho}}{M_{k,J}}, \quad \hat{u}_k = \frac{M_{k,J\rho u}}{M_{k,J\rho}}, \\ \hat{e}_k = \frac{M_{k,J\rho e}}{M_{k,J\rho}}, \quad \hat{\varepsilon}_k = \hat{e}_k - \frac{1}{2}(\hat{u}_k)^2. \end{cases} \tag{17}$$

For the pressure $\hat{P}_k$ and the sound speed components $\hat{c}_k$ one uses the equation of state and its derivatives:

$$\hat{P}_k = P(\hat{\rho}_k, \hat{\varepsilon}_k), \qquad \hat{c}_k = \sqrt{(\partial_\rho P)_S(\hat{\rho}_k, \hat{P}_k)}, \tag{18}$$

where $(\partial_\rho P)_S$ denotes the isentropic derivative of P. These results enable us to obtain the flux vector $F(\hat{\phi}_k)$. It remains the evaluation of the so-called star values of u and P. This procedure is described in the following section.

2.1.6. Riemann solver

At the beginning of each time step and for each node x_i we know the left and right states (ϕ_i^-, ϕ_i^+). One computes the intermediate state $\phi_i^\star$ by solving the Riemann problem which describes the evolution of initial discontinuities in the time interval Δt. In our code we use an approximate Riemann solver due to Godunov:

$$\begin{cases} u_i^\star = \frac{P_i^- - P_i^+ + \rho_i^+ c_i^+ u_i^+ + \rho_i^- c_i^- u_i^-}{\rho_i^+ c_i^+ + \rho_i^- c_i^-}, \\ P_i^\star = \frac{\rho_i^+ c_i^+ \rho_i^- c_i^- (u_i^- - u_i^+) + \rho_i^+ c_i^+ P_i^- + \rho_i^- c_i^- P_i^+}{\rho_i^+ c_i^+ + \rho_i^- c_i^-}, \end{cases} \tag{19}$$

where the left (right) state is determined by the hat components:

$$\phi_i^- = \hat{\phi}_K, \quad \text{in } \omega_{i-1/2}, \qquad \phi_i^+ = \hat{\phi}_0, \quad \text{in } \omega_{i+1/2}. \tag{20}$$

2.1.7. Time step controls

We have two limitations on the time step, the first one is the classical CFL condition and the second one ensures the positivity of the Jacobian J.

- CFL condition: we propose a heuristic CFL condition which seems to be convenient for almost all cases we have tested:

$$\Delta t_{\mathrm{CFL}} < \min_{i=1\ldots I}\left(\frac{\Delta x_{i+1/2}}{\frac{\hat{c}_0(i+1/2)}{\hat{J}_0(i+1/2)} + \frac{\hat{c}_K(i+1/2)}{\hat{J}_K(i+1/2)}}\right). \tag{21}$$

  It expresses the condition that in a given cell, two waves emanating from the boundaries x_i and x_{i+1} do not interact.
- Positivity of the Jacobian: the map between the Eulerian and the Lagrangian space remains valid as long as the Jacobian is strictly positive. In the case of compression, J is decreasing, so we have to ensure its positivity by a time step constraint. If moments of the Jacobian are positive at the beginning of each time step, they must remain so at the end of the time step, hence:

$$\Delta t_J < \min_{i=1\ldots I}\left[\min_{k=0\ldots K}\left(-\frac{M^n_{k,J}}{\sum_{l=0}^{K} D_{kl}\hat{u}^n_l - u^\star_{i+1}\delta_{kK} + u^\star_i\delta_{k0}}\right)\right]. \tag{22}$$

  Finally one takes the more restrictive condition by imposing:

$$\Delta t = \min(\Delta t_{\mathrm{CFL}}, \Delta t_J). \tag{23}$$

2.1.8. Eulerian grid computation

In order to represent the results in the physical space (namely the Eulerian space), one has to compute the time evolution of the Eulerian position X_i. For this purpose one solves the differential equation (Eq. (2)) following the two-step Runge–Kutta scheme:

$$\begin{cases} X_i^{(n,1)} = X_i^n + \Delta t u_i^\star, \\ X_i^{(n,2)} = X_i^{(n,1)} + \Delta t u_i^{\star(n,1)}, \\ X_i^{n+1} = \frac{1}{2}(X_i^{(n,2)} + X_i^n). \end{cases} \tag{24}$$

We represent the variable ϕ by its mean value $\bar{\phi}$ in each cell:

$$\begin{cases} \bar{\rho} = \frac{\sum_{k=0}^{K} M_{k,J\rho}}{\sum_{k=0}^{K} M_{k,J}}, \quad \bar{u} = \frac{\sum_{k=0}^{K} M_{k,J\rho u}}{\sum_{k=0}^{K} M_{k,J\rho}}, \\ \bar{e} = \frac{\sum_{k=0}^{K} M_{k,J\rho e}}{\sum_{k=0}^{K} M_{k,J\rho}}, \quad \bar{P} = \frac{\sum_{k=0}^{K} M_{k,J}\hat{P}_k}{\sum_{k=0}^{K} M_{k,J}}. \end{cases} \tag{25}$$

Remark 1. The method presented here allows to reach the spatial precision which is almost of the order of $K+1$, and the temporal precision of the order of 2. Notice that for $K=0$ it reduces to the classical Godunov Lagrangian scheme. For $K=1,2$ and for moderate compressive flows (no shocks), it works quite well, without any spurious oscillations, hence there is no need for the slope limitation procedure. Nonetheless, for strong compressive flows, one has to take account of the limitation procedure, in order to ensure monotonicity of the variables.

2.1.9. Numerical results

Fig. 1 shows the solution for the double expansion problem obtained with various numerical schemes. One clearly sees that none of the classical schemes reproduces the known analytical solution. Fig. 2 shows the re-

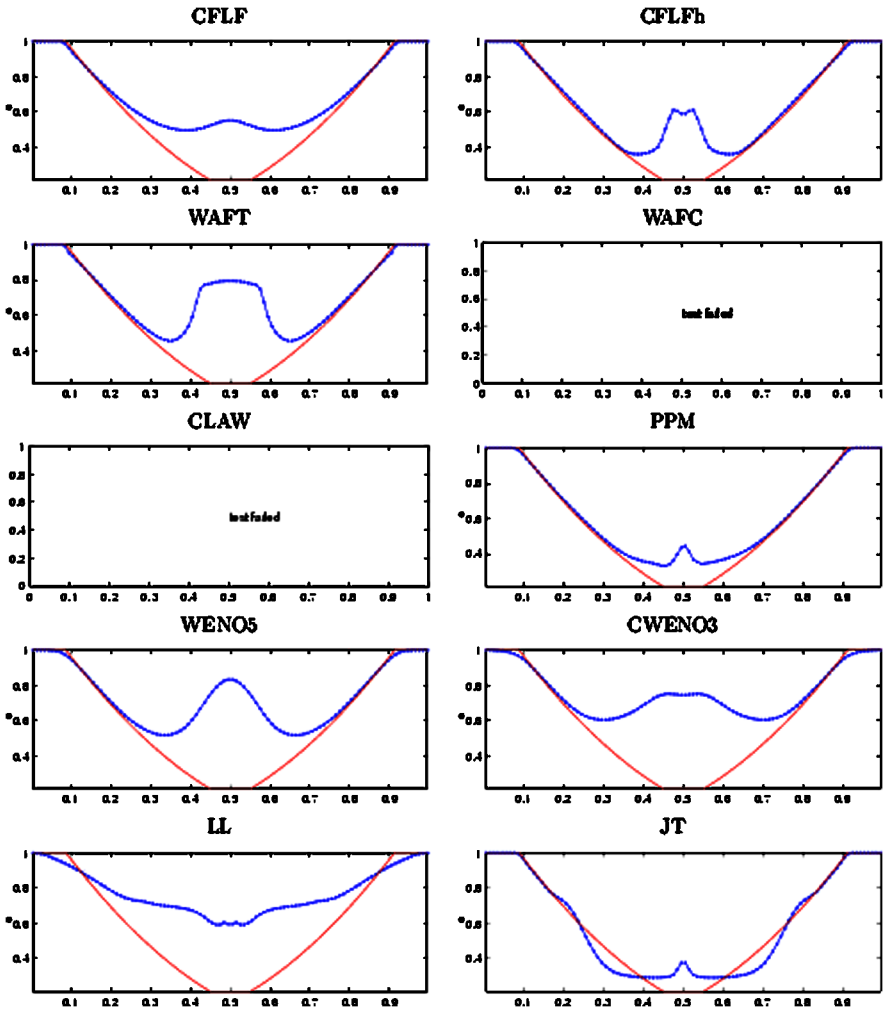

Fig. 1. Solution of the double expansion problem with various numerical schemes (taken from [13] where also a detailed explanation of the various numerical schemes is given), to be compared with Fig. 2. The grey curve gives the correct analytical solution and the dark ones the corresponding solutions of the various numerical schemes. No solution was obtained for the methods WAFC and CLAW. The abbreviations stand for: CFLF: a first-order Courant–Friedrichs–Lax–Friedrichs, CFLFh: CFLF hybrid, WAFT and WAFC: weighted average flux schemes, CLAW: clawpack wave propagation scheme, PPM: piecewise parabolic method, WEN05 and CWEN03: weighted essentially non-oscillatory schemes, LL: Liu–Lax positive scheme, JT: centered scheme with limiter.

sults from the Lagrangian discontinuous Galerkin method. Note that no numerical oscillations appear and that a moderate number of mesh points reproduces exactly the analytical result.

This particular test is related to the effect of a ponderomotive force acting on a plasma where a similar density depletion occurs and where very similar numerical problems play a role.

2.2. General outline of the method in 2D

The generalization of the Lagrangian discontinuous Galerkin method to the 2D geometry is rather straightforward but algebraically cumbersome. We present here only the main features. For a more detailed exposition

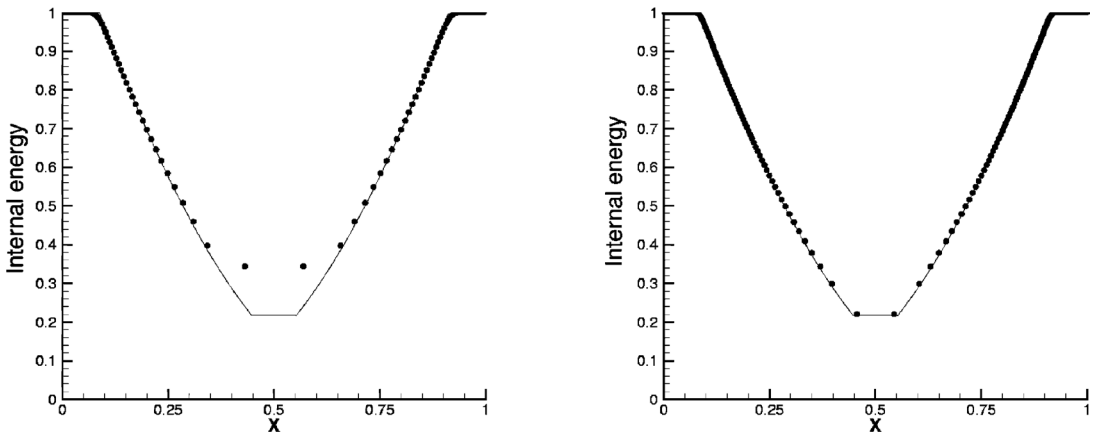

Fig. 2. The double expansion problem for the present numerical scheme (taken from [14]), using 100 (*left*) and 250 (*right*) computational cells. The continuous line gives the analytical solution and the dots represent the computational cell values.

the reader may refer to Ref. [15]. One of the particularities of the 2D numerical scheme relies on the expression of the gas dynamic equations in a conservation form in the Lagrangian framework as it was first pointed out in Ref. [12].

2.2.1. Gas dynamic equations in Lagrangian coordinates

Let Ω be an open set of $\mathbb{R}^2$, $\mathbf{X} = (X, Y)^t \in \Omega$ denotes the Eulerian coordinates in the flow field $\mathbf{V} = (u, v)^t$, and $\mathbf{x} = (x, y)^t$ denotes the Lagrangian coordinates which are the initial positions of the Eulerian coordinates (X, Y). The coordinates (X, Y) and (x, y) are connected by the system of ordinary differential equations:

$$\begin{cases} \partial_t X = u(X(t), Y(t), t), & \text{with } X(0) = x, \\ \partial_t Y = v(X(t), Y(t), t), & \text{with } Y(0) = y. \end{cases} \tag{26}$$

The solutions of Eq. (26) define a map between the Lagrangian and the Eulerian spaces for each time t. This map is bijective if and only if the associated Jacobian matrix is invertible. Hence its determinant J must be strictly positive (since it is positive at $t = 0$):

$$J(x, y, t) = \begin{vmatrix} \partial_x X & \partial_x Y \\ \partial_y X & \partial_y Y \end{vmatrix}. \tag{27}$$

The derivation of the gas dynamic equations in the Lagrangian space in the conservative form is based upon the following formula:

$$J \nabla_X \cdot \mathbf{F} = \nabla_x \cdot \big[f(\nabla_x Y)_\perp - g(\nabla_x X)_\perp \big]. \tag{28}$$

Here $\nabla_X \cdot$ denotes the divergence operator in Eulerian coordinates, $\nabla_x \cdot$ and ∇_x are the divergence and gradient operators in Lagrangian coordinates, $\mathbf{F} = (f, g)^t$, $(\nabla_x Y)_\perp = (-\partial_y Y, \partial_x Y)^t$ and $(\nabla_x X)_\perp = (-\partial_y X, \partial_x X)^t$. With these notations we obtain:

$$\begin{cases} \partial_t (J) - \nabla_x \cdot [u(\nabla_x Y)_\perp - v(\nabla_x X)_\perp] = 0, \\ \partial_t (\rho J) = 0, \\ \partial_t (\rho J u) + \nabla_x \cdot [P(\nabla_x Y)_\perp] = 0, \\ \partial_t (\rho J v) - \nabla_x \cdot [P(\nabla_x X)_\perp] = 0, \\ \partial_t (\rho J e) + \nabla_x \cdot [P u (\nabla_x Y)_\perp - P v (\nabla_x X)_\perp] = 0, \\ P = (\gamma - 1)\rho[e - \frac{1}{2}(u^2 + v^2)]. \end{cases} \tag{29}$$

2.2.2. The 2D numerical scheme

As in 1D, the 2D scheme is built with the discontinuous Galerkin method. We compute the moments of variables in the Bernstein polynomial basis. The mesh is nonstructured, using a triangulation of the set Ω. The construction of Bernstein polynomials on a triangle is straightforward, using the barycentric coordinates. We use the parabolic representation which enables us to obtain the spatial precision of the order of 3. Intermediate values on the triangle edges are evaluated with a monodimensional Riemann solver in the direction of the Eulerian outward unit normal vector. For the time discretization we have implemented a two-step Runge–Kutta method in order to obtain the temporal precision of the order of 2. A more complete description can be found in Ref. [14].

3. Formulation of the global model

3.1. Parabolic electromagnetic equation

The electromagnetic part of the code is based on the reduced, paraxial equation for the electromagnetic field amplitude. This is an envelope equation which accounts for a quasi-monochromatic laser field and its small divergence.

The time evolution of the electromagnetic field propagating in z-direction is given by the paraxial equation (19):

$$\left(2\imath\frac{\omega_o}{c^2}\partial_t + 2\imath k_o\partial_z + \imath\partial_z k_o + D^2 - \frac{\omega_o^2}{c^2}\frac{n_e - n_{eo}}{n_c} + \imath\frac{\nu_{ei}\omega_o}{c^2}\frac{n_{eo}}{n_c}\right)E = 0. \tag{30}$$

The operator $D^2 = 2\nabla^2/(1+\sqrt{1+\nabla^2/k_o^2})$, where ∇^2 is the Laplacian operator in the plane perpendicular to the z-direction, takes into account the Feit and Fleck correction [9] which allows to consider larger scattering angles. Here n_{eo} and n_e are the original and the actual electron density, respectively. The critical density is $n_c = m_e\epsilon_o\omega_o^2/e^2$, ω is the laser frequency and the wave vector is $k_o = (\omega_o/c)\sqrt{1-n_{eo}/n_c}$. ν_{ei} denotes the electron–ion collision frequency and this term accounts for depletion of the laser energy due to inverse bremsstrahlung.

This equation is common to all mesoscopic plasma models. It is solved by using the Fourier transform technique in the perpendicular plane as it was already described in Ref. [19]. The electromagnetic part of the code is supplemented by a package which allows for the use of the various schemes of optical smoothing as envisaged in the LMJ and NIF projects.

3.2. The non-local Navier–Stokes equations

Following the standard procedures to derive the moment equations from the Fokker–Planck equation for a plasma one arrives at the following set of hydrodynamic equations which has been derived in Ref. [3]:

$$\frac{\partial n_i}{\partial t} = -\nabla\cdot(n_i\mathbf{u}), \tag{31}$$

$$\begin{aligned}\frac{\partial \mathbf{u}}{\partial t} &= -(\mathbf{u}\cdot\nabla\mathbf{u}) - \frac{1}{n_i m_i}\nabla p_{\mathrm{tot}} - \frac{Z}{m_i}\frac{1}{2cn_c}\nabla I + \frac{1}{n_i m_i}\nabla\cdot(\eta_i\nabla\mathbf{u})\\ &\quad + \frac{Z}{m_i}\nabla(\beta T_e) - \frac{Z}{m_i}\frac{1}{cn_c}\nabla(\xi_u I) - \frac{Z}{m_i}\frac{1}{3cn_c}\nabla(\beta I),\end{aligned} \tag{32}$$

$$\begin{aligned}\frac{\partial T_e}{\partial t} &= -\frac{2}{3}T_e\nabla\cdot\mathbf{u} - \mathbf{u}\cdot\nabla T_e + \frac{2}{3n_c c}\nu_{ei} I + \frac{1}{3n_c c}\frac{\partial I}{\partial t} + \frac{2}{3}T_e\nabla\cdot(\beta\mathbf{u})\\ &\quad + \frac{2}{3n_e}\nabla\cdot(\kappa_e\nabla T_e) - \frac{2}{3}\nabla\cdot\left(\frac{\kappa_e}{3n_e n_c c}\nabla I\right) - \frac{2}{3}\nabla\cdot\left(\frac{T_e}{m_e\nu_{ei}n_c c}\xi\nabla I\right),\end{aligned} \tag{33}$$

$$\frac{\partial T_i}{\partial t} = -\frac{2}{3}T_i\nabla\cdot\mathbf{u} - \mathbf{u}\cdot\nabla T_i + \frac{2}{3n_i}\nabla\cdot(\kappa_i\nabla T_i), \tag{34}$$

$$p_{\text{tot}} = p_e + p_i, \tag{35}$$

$$p_e = (\gamma_e - 1) n_e \epsilon_e, \tag{36}$$

$$p_i = (\gamma_i - 1)\left(n_i \epsilon_i - \frac{1}{2} m_i n_i \mathbf{u}^2\right) \tag{37}$$

with ϵ_e, ϵ_i the total energy for electrons and ions, respectively.

Outwardly the structure of the equations is the same as in standard hydrodynamics. The difference being that the transport coefficients for viscosity and heat fluxes (η_i, κ_e and κ_i) have a non-local form as will be explained for the heat flux equation in the next section. In addition there are terms (containing the intensity $I = c\epsilon_o |E|^2/2$) which couple the plasma dynamics to the laser field.

This set of equations can be considered as non-local Navier–Stokes equations which take into account kinetic effects whenever the mean-free path for electron–ion collisions is of the order of the typical gradient scale lengths. The coupling terms due to inverse bremsstrahlung $(2/3n_c c)\nu_{ei} I + (1/3n_c c)\partial_t I$ and the ponderomotive force term $(Z/m_i 2cn_c)\nabla I$ remain purely local in character. The non-local transport coefficients will be explained in the following section.

4. The non-local transport

Under plasma conditions where the mean-free path for electron–ion collisions is of the order of the characteristic scale length of the macroscopic variables (density, temperature, etc.), the standard classical theory of transport breaks down. The classical transport is valid in the strongly collisional regime. It describes, for example, the heat flux by the well-known Spitzer–Härm formula. The weakly-collisional regime, characteristic for many laser–plasma interaction problems, requires a delocalized treatment of the transport coefficients, i.e. taking into account the variation of the plasma parameters on the scale of a few mean-free paths.

The model presented here is based on a mathematical exact linearization of the Fokker–Planck equation [2,3,5–7] and on an integral representation of the plasma fluxes and laser–plasma coupling. They are valid for an arbitrary collisionality and give a smooth transition from the collisional to the collisionless regime. Comparisons with kinetic calculations have shown that the so obtained formulae remain valid even under quasi-nonlinear conditions and can therefore be considered to be well adapted to the problems of interest [4]. Nonlinear models of the non-local transport have been developed only for the case without laser radiation and for a sufficiently strong collisionality [20]. Also they suffer from numerical problems when implemented in hydrodynamic codes. They can produce negative temperatures and negative entropy whenever the plasma density profile is non-uniform [8,18].

In the following we briefly present the procedure of implementation of the non-local heat flux in the code. All other transport coefficients are treated in exactly the same way from the mathematical point of view.

4.1. The electron heat conductivity

The simplified heat equation is (the temperature being in energy units [eV]):

$$\partial_t T_e = -\frac{2}{3n_e} \nabla \cdot \mathbf{q}. \tag{38}$$

The electron heat flux $\mathbf{q}$ has a non-local integral relation to the temperature gradient. Its Fourier component is $q_k = -\kappa_k (\nabla T)_k$ The electron heat conductivity κ_e is known in k-space but it is also a function of the local plasma parameters. As one is interested in conditions where the gradient scale length is of the order of the electron mean-free path, the Fourier component of the conductivity does not vary much over the gradient. One can therefore approximate the source $\nabla \cdot \mathbf{q}$ in Fourier space as $k^2 \kappa_k T_k$.

In the case of laser–plasma interaction, the laser intensity gradients are strongly anisotropic and are directed predominantly in the plane perpendicular to the laser propagation direction. This allows to consider the plasma response independently for each coordinate in the direction of laser beam propagation and therefore to limit the hydrodynamic equations to the 2D case. Correspondingly, the Fourier transformation of the heat flux is in 2D as well and one has $k^2 = k_x^2 + k_y^2$. The change in temperature at one time step is then given as:

$$\delta T_e = \frac{2\Delta t}{3n_e}\mathbf{FT}^{-1}\big[f_{nl}(k\lambda_{ei})\alpha k T_k\big]. \tag{39}$$

Here $\mathbf{FT}^{-1}$ denotes the inverse Fourier transform. Note that the coefficient $\alpha = n_e v_{Te}$ and the electron mean-free path λ_{ei} are given in real space and do not depend on k. The non-local transport coefficient f_{nl} is a nonlinear function of $k\lambda_{ei}$ which can be decomposed as:

$$f_{nl}(k\lambda_{ei}) = g(Z)k\lambda_{ei}h(k\lambda_{ei}), \tag{40}$$

with $g(Z) = (3.26 + 13.6Z)/(4.2 + Z)$ giving the ion charge dependence. If the function h is equal to 1, one would recover the standard expression for the collisional Spitzer–Härm conductivity: $\kappa = \kappa_{SH} = g(Z)n_e v_{Te}\lambda_{ei}$. In the general case the function h depends strongly on the collisionality parameter $k\lambda_{ei}$. It is possible to represent the function h as a harmonic mean between the strongly collisional h_c and the collisionless h_{nc} states which gives a good approximation over the whole range of the collisionality parameter X:

$$\frac{1}{h} = \frac{1}{h_c} + \frac{1}{h_{nc}}, \tag{41}$$

$$h_c = \frac{1}{1 + (\frac{50+10Z}{12+Z}X)^{0.9}}, \tag{42}$$

$$h_{nc} = \frac{0.11\sqrt{Z}}{X}, \tag{43}$$

with $X = \sqrt{Z}k\lambda_{ei}$.

Fig. 3 shows the strong variation of the electron heat flux coefficient as a function of the collisionality parameter $k\lambda_{ei}$ for various charge states and the relative importance of the collisional and collisionless contributions. Note that

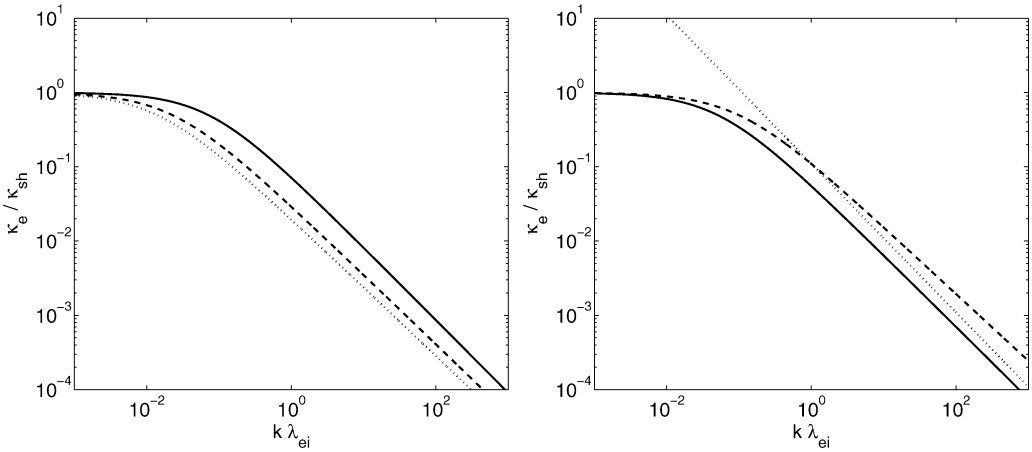

Fig. 3. *Left*: the non-local electron heat flux coefficient κ_e normalized to the Spitzer–Härm conductivity as a function of $k\lambda_{ei}$; solid line ($Z = 1$), dashed line ($Z = 20$) and dotted line ($Z = 50$). *Right*: the conductivity for $Z = 3.5$; solid line (h), dashed line (h_c) and dotted line (h_{nc}).

the transition from the collisional to the collisionless regime spans a wide range of parameters from $k\lambda_{ei} \approx 0.01$ to $k\lambda_{ei} \approx 100$.

Other transport coefficients are defined by the same interpolation formula, Eq. (41), with the following functions.

4.2. The ion heat conductivity

The change in the ion temperature at one time step is given as:

$$\delta T_i = (2\Delta t/3n_i)\mathbf{FT}^{-1}\left[f_{nl}(k\lambda_{ii})\alpha k T_k\right]$$

with $\alpha = n_i v_{Ti}$ and the function $f_{nl}(k\lambda_{ii}) = k\lambda_{ii}h(k\lambda_{ii})$ is defined according to Eq. (41) with

$$h_c = 2.78; \quad h_{nc} = \frac{\sqrt{\pi}}{8}\frac{\mathrm{e}^{-(\frac{1}{Y}+3)/2}}{Y^3 X}$$

with $X = k\lambda_{ii}$ and $Y = T_i/ZT_e$ and the Braginskii viscosity being: $\kappa_{oi} = 2.78 n_i v_{Ti}\lambda_{ii}$.

4.3. The ion viscosity

The change in the ion velocity due to viscosity can be written as:

$$\delta u = \frac{\Delta t}{n_i}\mathbf{FT}^{-1}\left[f_{nl}(k\lambda_{ii})\alpha k u_k\right]$$

with $\alpha = n_i v_{Ti}$ and $f_{nl}(k\lambda_{ii}) = k\lambda_{ii}h(k\lambda_{ii})$, where

$$h = 2.0\frac{1.48 + 0.8Y^2}{2.31 + 4.04Y^2 + Y^4}; \quad Y = k\lambda_{ii}/\sqrt{\frac{T_i}{ZT_e}},$$

to which is added the ion Landau damping:

$$h_{\text{landau}} = \sqrt{\pi/8}\left(\frac{T_i}{ZT_e}\right)^{-1.5}\sqrt{3 + \frac{ZT_e}{T_i}}\mathrm{e}^{-1.5+\frac{ZT_e}{2T_i}}\left[\frac{14(k\lambda_{ii})^2}{1 + 7(k\lambda_{ii})^2}\right].$$

4.4. The coefficients β, ξ and ξ_u

The collisional (c) and collisionless (nc) limits of these coefficients are given by the following equations:

$$\beta = \begin{cases} \frac{150X^2/Z}{1+2.8(1+12X/\sqrt{Z})(\frac{-5+10Z}{7+Z}X)^{0.9}} & \text{coll.,} \\ 0.4 & \text{non-coll.,} \end{cases}$$

$$\xi = \begin{cases} 34.5\frac{Z}{1+37X^{1.34}} & \text{coll.,} \\ 1.3\frac{Z^{1.5}}{X^{1.57}} & \text{non-coll.,} \end{cases}$$

$$\xi_u = \begin{cases} 180\frac{X^2}{1+42(1+12X/\sqrt{Z})X^{1.3}} & \text{coll.,} \\ 0.34\frac{Z}{X^{0.57}} & \text{non-coll.} \end{cases}$$

As before the interpolation formulae for the above coefficients use the harmonic mean. For example, one has: $\frac{1}{\beta} = \frac{1}{\beta_{\text{c}}} + \frac{1}{\beta_{\text{nc}}}$.

For all transport terms one has that in the limit of $k\lambda_{ei} \to 0$ the standard collisional transport is recovered automatically. However, the non-local Navier–Stokes equations are valid for arbitrary collisionality of the plasma, from the free-streaming limit via the semi-collisional regime to the usual strongly collisional regime.

4.5. Implicit treatment of the heat flux term

The heat flux $\mathbf{q} = -\kappa_e \nabla T_e$ poses numerical stability problems. There is a general disparity for the characteristic propagation velocity of a density perturbation which is of the order of the ion sound velocity $c_s \sim \sqrt{T_e/m_i}$ and the characteristic speed for a thermal wave which is $v_{\text{th}} \lesssim \sqrt{T_e/m_e}$ (depending on the model). These two velocities differ by two orders of magnitude due to the large difference between the ion mass m_i and the electron mass m_e. This introduces a two-scale problem for the time step for integration.

In these conditions it is necessary to use an implicit treatment of the non-local transport term.

In the explicit version the heat conduction term in Eq. (38) was evaluated at the time step n following Eq. (39) with T_k taken at the same time step n. In a generalized implicit spectral treatment the starting point is:

$$n_e(x)\frac{T_k^{n+1} - T_k^n}{\Delta t} = A\left\{\theta T_k^{n+1} + (1-\theta)T_k^n\right\}, \tag{44}$$

with $A = -k^2\kappa_k(k\lambda_{ei}(x))\frac{2}{3}n_e(x)v_{Te}(x)/\Delta t$ and θ is a positive parameter which lies between 0 and 1. The new temperature is then calculated as:

$$T_k^{n+1} = T_k^n \frac{n_e(x) + A(1-\theta)}{n_e(x) - A\theta}. \tag{45}$$

For $\theta = 0$ the scheme is explicit, for $\theta = 1$ it is purely implicit. For $\theta = \frac{1}{2}$ we recover the semi-implicit Crank–Nicholson scheme.

Subsequently the new temperature is obtained as $T^{n+1}(x) = \mathbf{FT}^{-1}[T_k^{n+1}]$ or with the correction term $\Delta T(x) = \mathbf{FT}^{-1}[T_k^{n+1} - T_k^n]$.

As the non-local transport theory is linearized in Fourier space, no matrix inversion is required for the implicit approach as each Fourier component is evaluated separately.

5. Nonlinear evolution stage of mono-speckles in LPI

The spatial and temporal smoothing of laser beams in plasmas plays an important role in inertial confinement fusion. The aim is to reduce the intrinsic intensity fluctuations in a laser beam which affect the compression uniformity of the pellet. Of particular interest is the plasma-induced temporal incoherence. One of the mechanisms playing a role is an intensity-dependent instability of a mono-speckle. This instability was successfully analyzed and validated in the linear regime by comparing it to analytical considerations and to experimental data [16]. As the plasma response at high intensities becomes nonlinear, the full nonlinear hydrodynamics is needed in order to correctly model the interaction process.

As was shown already in the linear response regime [16], the intrinsically non-local character of the transport terms may not be neglected. In the following nonlinear calculation they were taken into account.

Fig. 4 shows the time evolution of the density of a mono-speckle in the strongly nonlinear regime. As the intensity of the laser beam is above a certain threshold a hose-like instability develops which eventually destroys the speckle in the plasma. This so-called filament instability is an important mechanism of plasma-induced smoothing for laser beams in the inertial confinement fusion applications. The onset of the instability is determined by the self-focusing of a laser beam in a plasma and the density fluctuations always present. Fig. 5

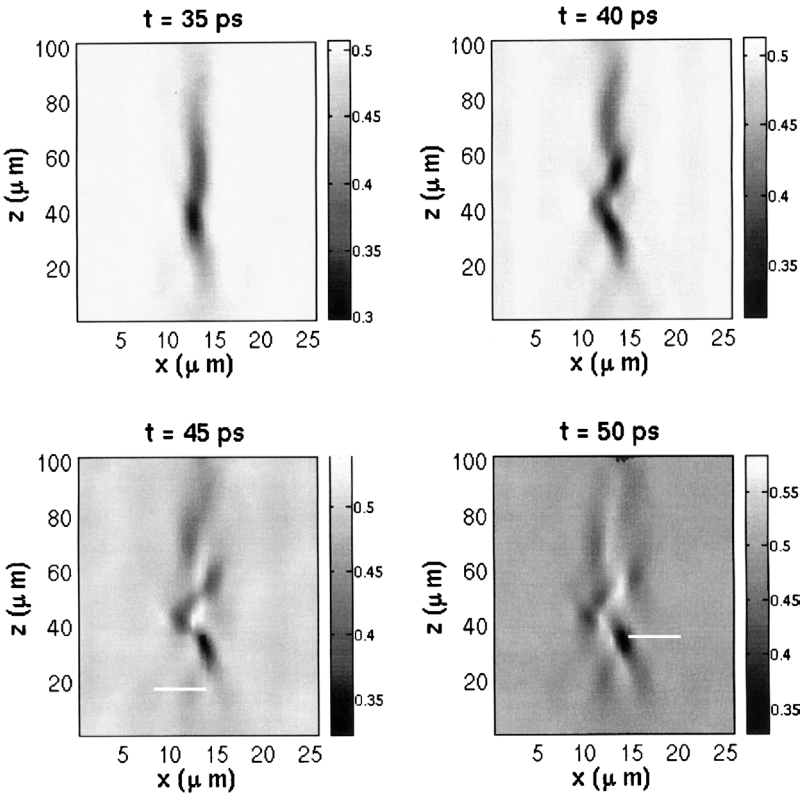

Fig. 4. Density plots of the nonlinear evolution of a mono-speckle around the time of destruction (plasma density: $n_e = 0.5\, n_c$ and the laser intensity: $8 \cdot 10^{13}$ W/cm^2); z-direction is parallel to the laser beam axis and x-direction is one of two transverse directions.

shows some snapshots of the corresponding evolution of the laser beam intensity up to the destruction of the speckle.

Fig. 6 shows the time evolution of a characteristic parameter linked to the behavior of the electromagnetic energy for the speckle instability. This is the relative part of the computational volume where the laser intensity exceeds three times the maximum laser intensity in the entrance plane. It characterizes the local concentration of the laser energy in the plasma due to self-focusing. The linear regime of this instability had been analyzed in [16] where it was found that this parameter exhibits an oscillatory behavior. This corresponds to a periodic reconstruction of the speckle and the instability mechanism repeats itself. For the higher laser intensity, the plasma response is nonlinear and we found that the instability changes its character completely. One no longer observes a periodic reconstruction of the speckle. This is an important result for the plasma smoothing which can be verified in experiments.

The modeling of large-scale plasmas requires the use of parallel machines. The code has been entirely parallelized using MPI [11] and the FFTW package [10] for the fast Fourier transforms which admits the use of MPI. The nonlinear calculation was performed for a plasma volume of $25 \times 25 \times 100$ μm^3 and for a duration of 150 ps. Using a transverse spatial resolution of 0.4 μm, a longitudinal spatial resolution of 1 μm (i.e. $64 \times 64 \times 100$ mesh points) and a time step for integration of $2.5 \cdot 10^{-2}$ ps (the small time step is mainly imposed by the explicit scheme and the coupling with the non-local transport terms) the entire calculation took of the order of 20 h on the equivalent of one processor on a Compaq hp alpha server machine.

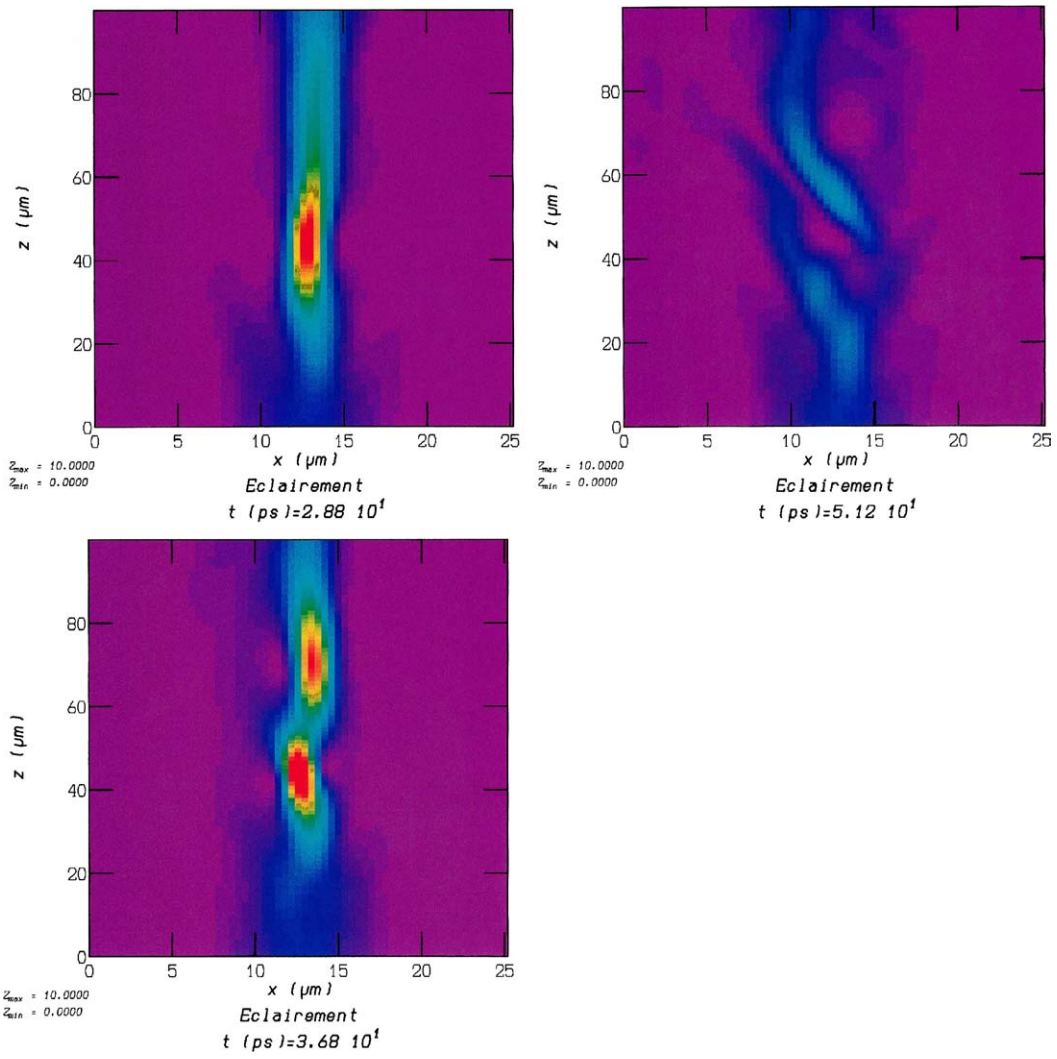

Fig. 5. Intensity plots of the nonlinear evolution of a mono-speckle. *Upper left*: initial stage of instability ($t = 28$ ps), lower left: hose-like instability ($t = 36.8$ ps) and *upper right*: destruction of the speckle ($t = 51.2$ ps).

6. Conclusion

We have presented a new mesoscopic code for modeling the laser–plasma interactions in the ICF context. The special feature of the code is a new numerical approach to describe the nonlinear plasma response. Although the discontinuous Galerkin method in the Lagrangian framework is more time-consuming than standard numerical approaches for hydrodynamics, this is more than compensated through the reduction of mesh points required, the absence of numerical oscillations and of limiting procedures (except for strong shocks), and a high precision. This approach seems to be very well adapted for rendering the nonlinear plasma response in LPI calculations.

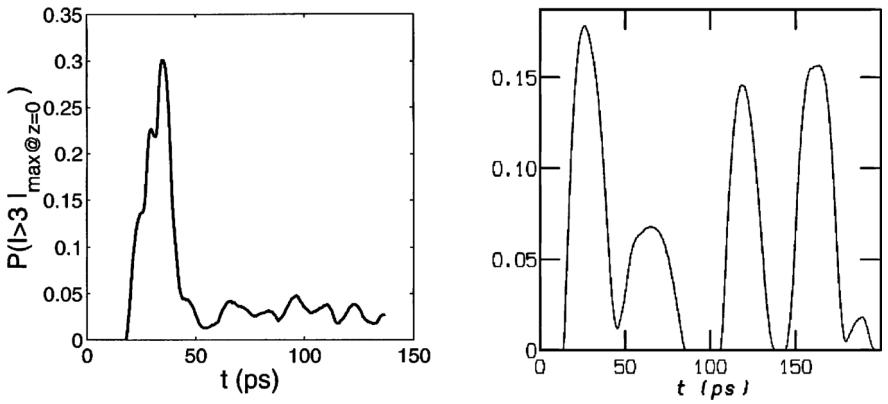

Fig. 6. Temporal evolution of the electromagnetic energy in the computational volume with the local intensity exceeding three times the maximum intensity in the plane of incidence. *Left*: a typical nonlinear case with the plasma density $n_e = 0.5\,n_c$ and the laser intensity $8 \cdot 10^{13}$ W/cm^2. *Right*: a representative linear case with the density $n_e = 0.2\,n_c$ and the intensity $3.6 \cdot 10^{13}$ W/cm^2 (taken from Ref. [16]).

Acknowledgements

The authors would like to thank O. Bertrand who was responsible for the parallelization of the code.

References

[1] R.L. Berger, C.H. Still, E.A. Williams, A.B. Langdon, On the dominant and subdominant behavior of stimulated Raman and Brillouin scattering driven by nonuniform laser beams, Phys. Plasmas 5 (1998) 4337.
[2] A.V. Brantov, V.Yu. Bychenkov, V.T. Tikhonchuk, Non-local plasma electron hydrodynamics, JETP 83 (1996) 716.
[3] A.V. Brantov, V.Yu. Bychenkov, V.T. Tikhonchuk, W. Rozmus, Non-local electron transport in laser heated plasmas, Phys. Plasmas 5 (1998) 2742.
[4] S. Brunner, E. Valeo, Simulations of electron transport in laser hot spots, Phys. Plasmas 9 (2002) 923.
[5] V.Yu. Bychenkov, J. Myatt, W. Rozmus, V.T. Tikhonchuk, Quasihydrodynamic description of ion acoustic waves in a collisional plasma, Phys. Plasmas 1 (1994) 2419.
[6] V.Yu. Bychenkov, W. Rozmus, V.T. Tikhonchuk, Non-local electron transport in a plasma, Phys. Rev. Lett. 75 (1995) 4405.
[7] V.Yu. Bychenkov, V.N. Novikov, V.T. Tikhonchuk, Theory of non-local transport for small perturbations in a plasma, JETP 87 (1998) 916.
[8] J. Delettrez, Thermal electron transport in direct-drive laser fusion, Can. J. Phys. 64 (1986) 932.
[9] M.D. Feit, J.A. Fleck, Beam nonparaxiality, filament formation and beam breakup in the self-focusing of optical beams, J. Opt. Soc. Am. B 5 (1988) 633.
[10] M. Frigo, S.G. Johnson, FFTW User's Manual, version 2.1.3, http://www.fftw.org, November (1999).
[11] W. Gropp, E. Lusk, User's Guide for MPICH, version 1.2.2, Argonne National Laboratory, ANL/MCS-TM-ANL-96/6 Rev. D, 1996.
[12] W.H. Hui, P.Y. Li, Z.W. Li, A unified coordinate system for solving the two-dimensional Euler equations, J. Comput. Phys. 153 (1999) 596.
[13] R. Liska, B. Wendroff, Comparison of several difference schemes on 1D and 2D test problems for the Euler equations, Conservation Law Preprint server, http://www.math.ntnu.no/conservation/, 2001.
[14] R. Loubère, Une méthode particulaire lagrangienne de type Galerkin Discontinu. Applications à la mécanique des fluides et l'interaction laser/plasma, PhD Thesis, Université Bordeaux, 1 2002.
[15] R. Loubère, J. Ovadia, R. Abgrall, A Lagrangian discontinuous Galerkin-type method on unstructured meshes to solve hydrodynamics problems, Int. J. Numer. Meth. Fluids 44 (2004) 645.
[16] P. Michel, C. Labaune, S. Weber, V.T. Tikhonchuk, G. Bonnaud, G. Riazuelo, F. Walraet, Studies of the laser filament instability in a semicollisional plasma, Phys. Plasmas 10 (2003) 3545.
[17] J. Myatt, A.V. Maximov, R.W. Short, Modelling laser–plasma interaction physics under direct-drive inertial confinement fusion conditions, LLE Rev. 91 (2002) 93.
[18] M.K. Prasad, D.S. Kershaw, Nonviability of some non-local electron heat transport modeling, Phys. Fluids B 1 (1989) 2430.

[19] G. Riazuelo, G. Bonnaud, Coherence properties of a smoothed laser beam in a hot plasma, Phys. Plasmas 7 (2000) 3841.
[20] G. Schurtz, P. Nicolaï, M. Busquet, A non-local electron conduction model for multidimensional radiation hydrodynamics codes, Phys. Plasmas 7 (2000) 4238.
[21] S. Weber, G. Riazuelo, P. Michel, R. Loubère, F. Walraet, V.T. Tikhonchuk, V. Malka, J. Ovadia, G. Bonnaud, Modelling of laser–plasma interaction on hydrodynamic scales: physics development and comparison with experiments, Laser Part. Beams 22 (2004) 189.